Soil Dynamics and Earthquake Engineering xxx (xxxx) xxx–xxx

Contents lists available at ScienceDirect

Soil Dynamics and Earthquake Engineering

journal homepage: www.elsevier.com/locate/soildyn

Kyoto University LEAP-GWU-2015 tests and the importance of curving the ground surface in centrifuge modelling

Tetsuo Tobita[a,*], Takayuki Ashino[b], Jianfei Ren[b], Susumu Iai[c]

[a] Faculty of Environmental and Urban Engineering, Kansai University, Japan
[b] Graduate School of Engineering, Kyoto University, Japan
[c] Disaster Prevention Research Institute, Kyoto University, Japan

ARTICLE INFO

Keywords:
Centrifuge modelling
LEAP-GWU-2015
Liquefaction
Radial gravity

ABSTRACT

This paper presents a description of testing procedure and results of the LEAP-GWU-2015, and an investigation of the effect of the radial gravity field in centrifuge modelling. Dynamic responses of two models are compared. One had a planar surface with a 5° slope relative to the base of the container; the other had a curved surface to maintain a constant slope angle with respect to the radial g-field. For the centrifuge tests employed in this study, the slope and base excitation are in the tangential direction to spinning centrifuge. Results show that spikes in acceleration records due to cyclic mobility associated with lateral displacements appeared on both models. However, for the plane surface model, acceleration spikes in the negative (upslope) direction are more prominent and the residual downslope ground deformation was larger. Larger lateral displacement was observed in the plane model, while surface displacements in the curved model are smaller and uniform along the length of the model. For the plane model, the radial gravity acting near the slope top is almost constant and gradually increases towards the slope toe which causes a net increase in effective slope angle. Curving the model ground surface is recognized as leading to uniform lateral displacements along the length of the model surface.

1. Introduction

The goal of this study is to visualize and evaluate the effect of radial gravity for two well-defined sloping model tests. The tests were part of the LEAP-GWU-2015 project [1]. A series of centrifuge model testing was conducted under the specific model setup provided by the organizer. The geotechnical centrifuge employed in this study is the one in the Disaster Prevention Research Institute, Kyoto University (DPRI-KU), in which the longer side of a sand box is placed tangential to the arm rotation circle. Firstly, we describe the model preparation procedure and specifications of the sensors for future references. Secondly, results of the two model tests are compared to illustrate the effect of radial gravity. In centrifuge model testing, it is a physical restriction that the centrifugal acceleration or gravity field in a model ground is radial. Because variation of the centrifugal acceleration on the surface is small when the arm length is large, the effect is usually assumed to be minor [2]. Under such a condition, the effect is usually ignored and results are interpreted as if the prototype ground surface is flat. However, if the arm length is short a planer surface simulates a curved surface in prototype. The effect may be more prominent under extreme conditions such as liquefaction.

To conclude the VELACS project, Scott [4] emphasized that the issue of quality control in physical modelling had to be clarified before moving on to a next step. This is still true after 20 years. Although the effect of the radial gravity is well known among physical modelers, these effects have been hardly reported and kept abstract. This study discusses these effects in particular to dynamic problems with well-defined saturated sloping ground, and finally confirms the importance of curving the ground surface in centrifuge modelling.

2. Model preparation

A beam centrifuge with a radius of 2.5 m is utilized in DPRI-KU. A shaking table is mounted on a swinging platform attached on the arm. The shaking direction is tangential to the arm rotation. By the specification given by the LEAP organizing committee (summarized by [1]) (Fig. 1), the centrifugal acceleration is determined to be 44.4 G with a sand box whose inner dimension is 45 × 15 × 30 (cm). In this study, the tests were carried out for two types of the sloping model ground, i.e., curved [Fig. 1(a)] and plane [Fig. 1(b)]. The curved surface model was the condition specified by the organizing committee for the type of centrifuge similar to DPRI-KU. A model test with a plane surface was

* Corresponding author.
E-mail address: tobita@kansai-u.ac.jp (T. Tobita).

https://doi.org/10.1016/j.soildyn.2018.05.005
Received 20 September 2015; Received in revised form 25 April 2018; Accepted 4 May 2018
0267-7261/ © 2018 Elsevier Ltd. All rights reserved.

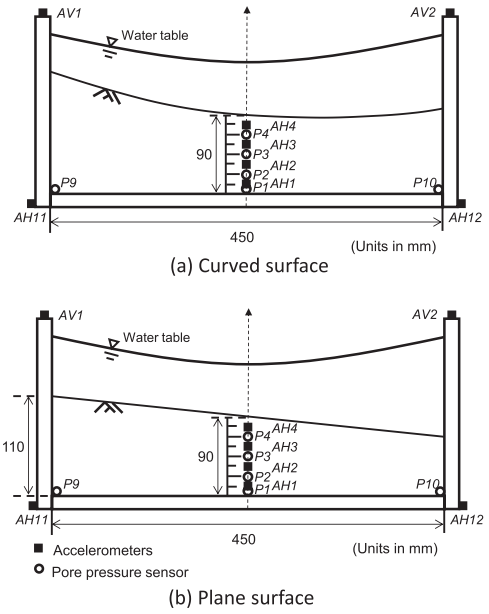

Fig. 1. Specified model ground and sensor locations (Model scale): (a) Curved surface and (b) Plane surface.

conducted additionally to evaluate the importance of the curvature of the surface.

Model ground was constructed by the sand pluviation method with the device shown in Fig. 2. Before making the model ground, calibration to obtain the density of 1652 kg/m^3 (relative density of 65%) for Ottawa F65 sand [G_s = 2.673, e_{max} = 0.76 (ρ_{min} = 1519 kg/m^3), e_{min} = 0.54 (ρ_{max} = 1736 kg/m^3)] was made by changing the pluviation height. After placing sensors (accelerometers and pore water pressure transducers) at the specified locations (Fig. 1), the sand was carefully pluviated in a rigid sandbox to make a flat ground surface. In this process, the density is assumed to be well controlled to have a specified value. Then, with a stainless tube (length = 0.6 m, outer diameter = 13 mm, wall thickness = 1 mm) connected with a vacuum, sand on the surface of the ground was carefully removed to shape the curved or plane surface (Fig. 3). By this method, only sand particles near the ground surface were carefully removed and disturbance on density of the model ground was minimized. The shape of the curved surface model was determined by tilting the mold of Fig. 3 at 5 °, whose top edge is cut to form a circular arc corresponding to a radius of 2.5 m. After placing surface displacement markers, which are a head of nylon cable ties, with approximate 2.3 cm spacing (1 m by 1 m in prototype scale), the sand box was put into a vacuum chamber for saturation (Fig. 4).

In the saturation process, firstly the air in the chamber was replaced

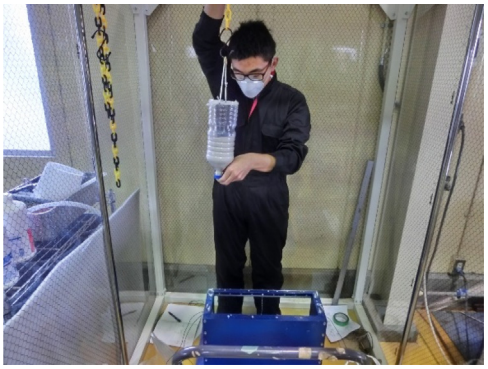

Fig. 2. Construction of model ground by sand pluviation method. Height of outlet was determined by calibration.

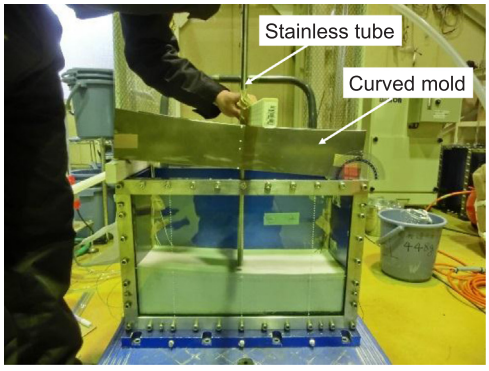

Fig. 3. Inclined curved surface was made by removing sands with a stainless tube attached to a vacuum. Height of the suction opening was adjusted by the mold whose top edge was curved with a circular arc with 2.5 m radius.

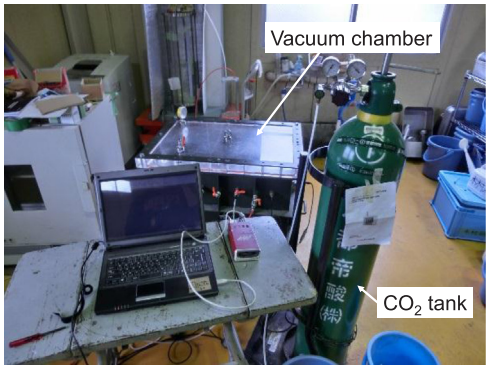

Fig. 4. Vacuum chamber and CO_2 tank.

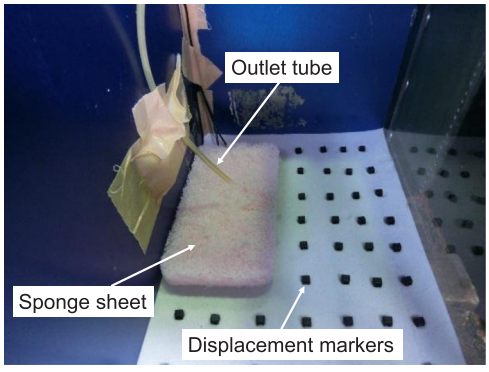

Fig. 5. Ground saturation procedure in a vacuum chamber. Viscous water is dropped from an outlet tube. A sponge sheet to protect the sand surface is carefully placed on the model ground.

with CO_2 gas. Then, vacuum close to − 0.1 MPa was applied. After such a high vacuum was achieved, a viscous fluid was dropped through a tube fixed near the surface of the model ground (Fig. 5). To minimize surface disturbance by the dropping fluid, the surface was protected by a sponge sheet (Fig. 5). The time required for full saturation was more than 10 h. The degree of saturation was measured by the vacuum chamber method [3]. In this model test, saturation degree as high as 99.9% was achieved. A solution of Methylcellulose (SM-100, Shin'etsu Chemical Co.) and water was used as a viscous fluid. Obtained viscosity versus temperature curve is shown in Fig. 6. Fluid temperature before and after the test of the curved surface were, respectively, 12.3 °C and 15.8 °C. Thus from Fig. 6, viscosity was estimated to be between 52.6 cSt and 47.2 cSt, slightly higher than the target (44.4 cSt).

After the saturation process (Fig. 7), the weight of the sandbox was

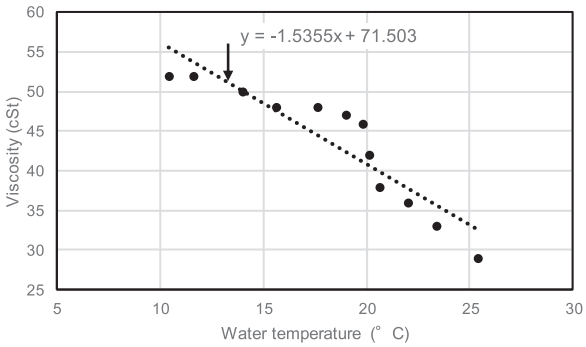

Fig. 6. Viscosity versus temperature relation of the curved model.

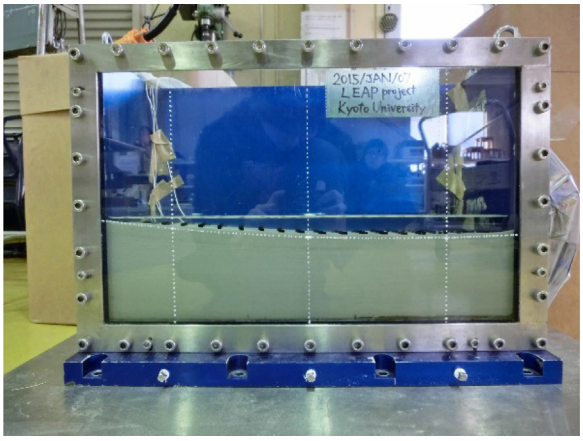

Fig. 7. Curved surface model after the saturation process.

measured to determine the mass of the counter balance-weight of the centrifuge arm. Then the box was fixed on the shaking table on the platform. The model ground was shaken 5 times with the specified motions (Table 1).

The hydraulic actuator of the shaker in DPRI-KU is controlled

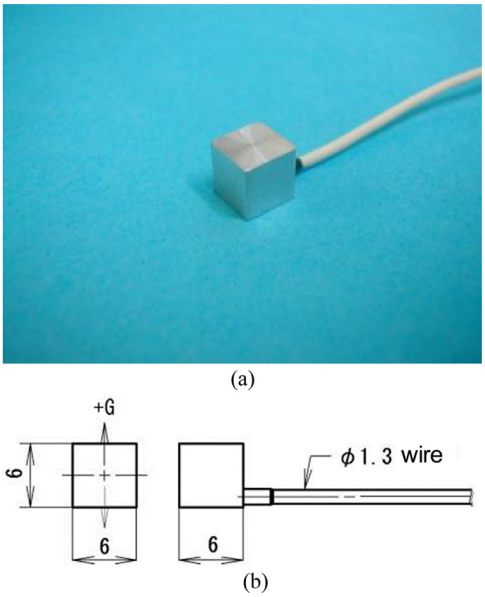

Fig. 8. External view of the accelerometer, A6H-50 (a) and dimension (scale in mm) (b).

Table 2
Specification of accelerometer and pore pressure transducer.

Type	A6H-50	P306A-2
Capacity	± 50 g	200 kPa
Output voltage	100mVRO	100mVRO
Overload	200%RO	150%RO
Non-linearity (& hysteresis)	1%RO	0.5%RO
Reproducibility	0.2%RO	0.2%RO
Temperature characteristic	0.05%RO/°C (0–40 °C)	0.05%RO/°C (0–40 °C)
Operating temperature range	− 10 °C to + 55 °C	− 10 °C to + 55 °C
Input/Output resistance	500 Ω	500 Ω
Bridge voltage	6VDC (8VDC MAX)	6VDC (8VDC MAX)

Table 1
(a) Event records for the test with curved surface and plane surface.

Event Number	Date	Description	Achieved Base Acc. (g_prototype scale)
Curved surface			
DPRI_01_1	2015/01/07	*Measure surface markers*	–
DPRI_01_2		*Spin up centrifuge*	–
DPRI_01_3		*CPT*	NA
DPRI_01_4		*Shake #1 ramped sine 1H, 0.015g*	0.010
DPRI_01_5		*Shake #2 ramped sine 1H, 0.15g*	0.148
DPRI_01_6		*Spin down*	–
DPRI_01_7		*Measure surface markers*	–
DPRI_01_8		*Shake #3 ramped sine 1H, 0.015g*	0.011
DPRI_01_9		*Shake #4 ramped sine 1H, 0.25g*	0.258
DPRI_01_10		*Shake #5 ramped sine 1H, 0.015g*	0.015
DPRI_01_11		*Spin down*	–
DPRI_01_12		*Measure surface markers*	–
Plane surface			
DPRI_02_1	2015/01/09	*Measure surface markers*	–
DPRI_02_2		*Spin up centrifuge*	–
DPRI_02_3		*CPT*	NA
DPRI_02_4		*Shake #1 ramped sine 1H, 0.015g*	0.010
DPRI_02_5		*Shake #2 ramped sine 1H, 0.15g*	0.149
DPRI_02_6		*Spin down*	–
DPRI_02_7		*Measure surface markers*	–
DPRI_02_8		*Shake #3 ramped sine 1H, 0.015g*	0.012
DPRI_02_9		*Shake #4 ramped sine 1H, 0.25g*	0.260
DPRI_02_10		*Shake #5 ramped sine 1H, 0.015g*	0.015
DPRI_02_11		*Spin down*	–
DPRI_02_12		*Measure surface markers*	–

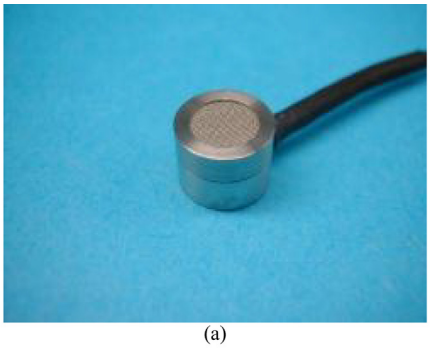

(a)

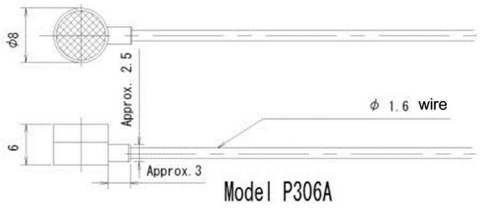

(b)

Fig. 9. External view of the pore water pressure transducer, P306A (a) and dimension (scale in mm) (b). A metal mesh filter covers a diaphragm.

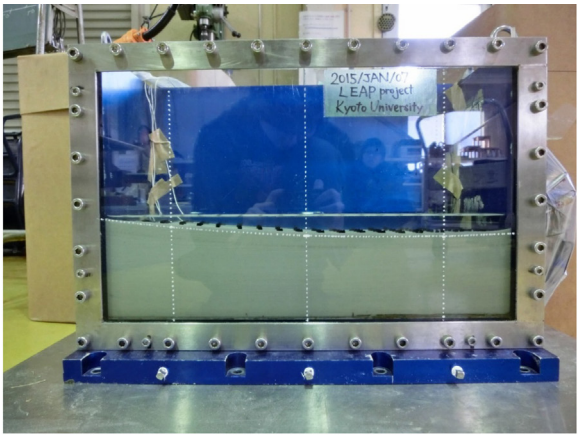

(a) Before mounting on the platform

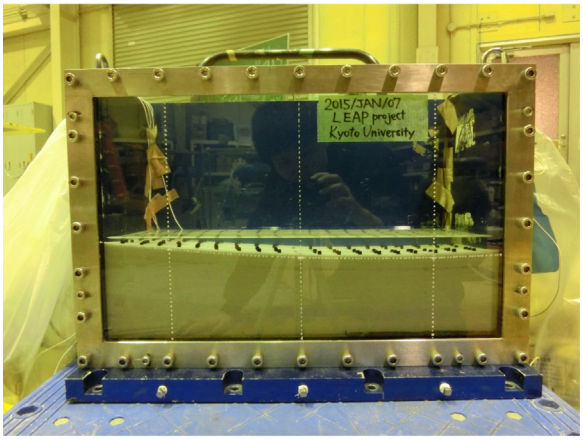

(b) After the test

Fig. 10. View of the curved surface model (a) before and (b) after a series of shaking.

through a set of servo-valves. The input signal is given by a time series of displacements (at full capacity: ± 5.0 mm). According to the specification of the shaker provided by the manufacturer, the achieved

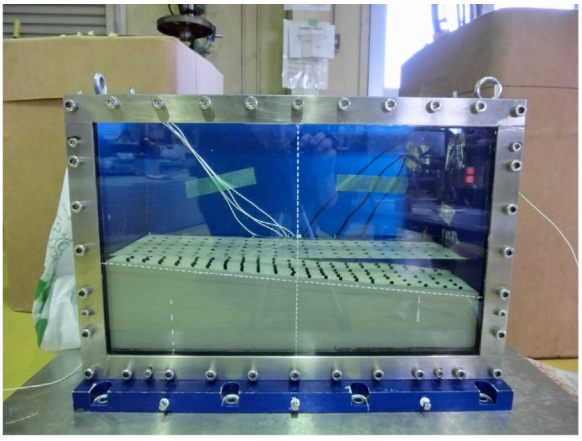

(a) Before mounting on the platform

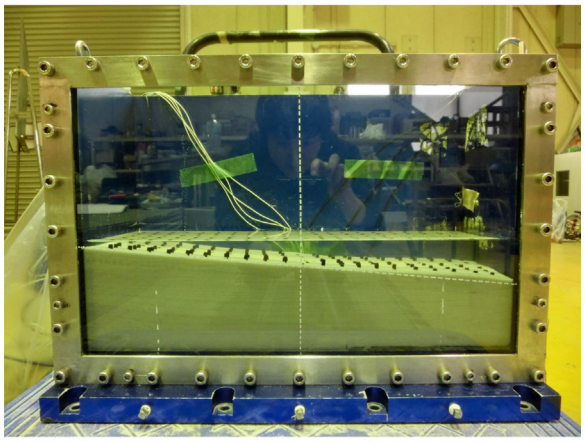

(b) After the test

Fig. 11. View of the plane surface model (a) before and (b) after a series of shaking.

maximum acceleration is 50 G, and the maximum frequency is 200 Hz under 100 kgf of an overburden load at 1 G field.

3. Sensors

As shown in Fig. 1, 6 accelerometers are installed at the specified positions. The accelerometer model is A6H-50 (SSK Co., Ltd.) (Fig. 8) with characteristics shown in Table 2. To minimize the settlement of accelerometers during shaking, a plastic sheet (1.5 × 1.5 cm) is glued at the base of the sensor. Then, sensor cables are attached on the side wall of the sandbox. After placing them on dry sand, they are immediately covered by a scoop of sand to fix their position. Sensors AV1 and AV2 are glued at the top of the walls of the sandbox.

Before sand pluviation, 6 pore water pressure transducers are also installed at the specified positions (Fig. 1), i.e., GL. − 1, − 2, − 3, and − 4 m (prototype scale). The model P306A-2 (SSK, Co., Ltd.) (Fig. 9) whose specification is given in Table 2 are employed. Unlike accelerometers, these sensors were attached at the back side of the sandbox with a water resistant double-stick tape so that their position would not vary during the experiment. It should be noted that for tests performed at other facilities in LEAP-GWU-2015, the pore pressure sensors were embedded in the sand and they would be expected to move with the sand during the experiment.

4. Test results

A side view of the sloping ground model with curved surface before and after the whole series of shaking sequence are shown in Fig. 10(a)

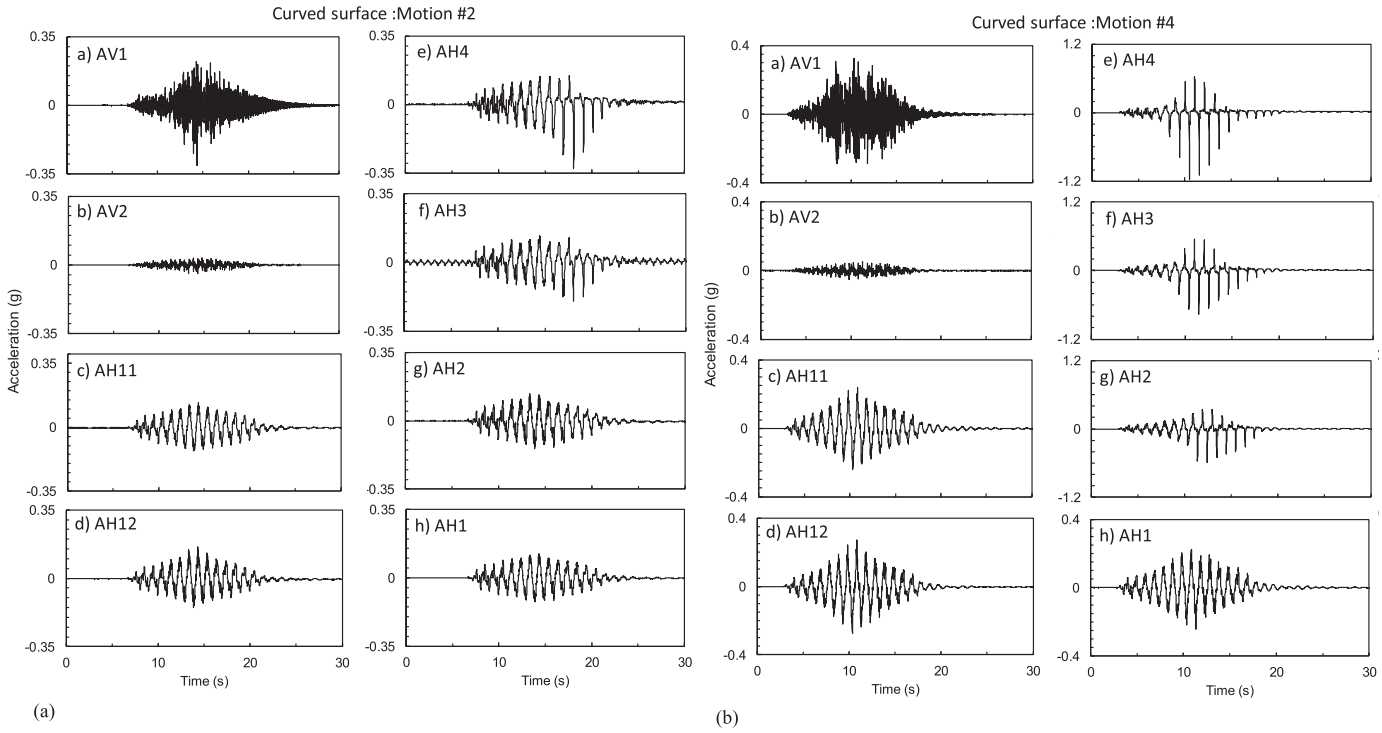

Fig. 12. (a) Recorded accelerations in Motion #2 for the curved surface model. (b) Recorded accelerations in Motion #4 for the curved surface model.

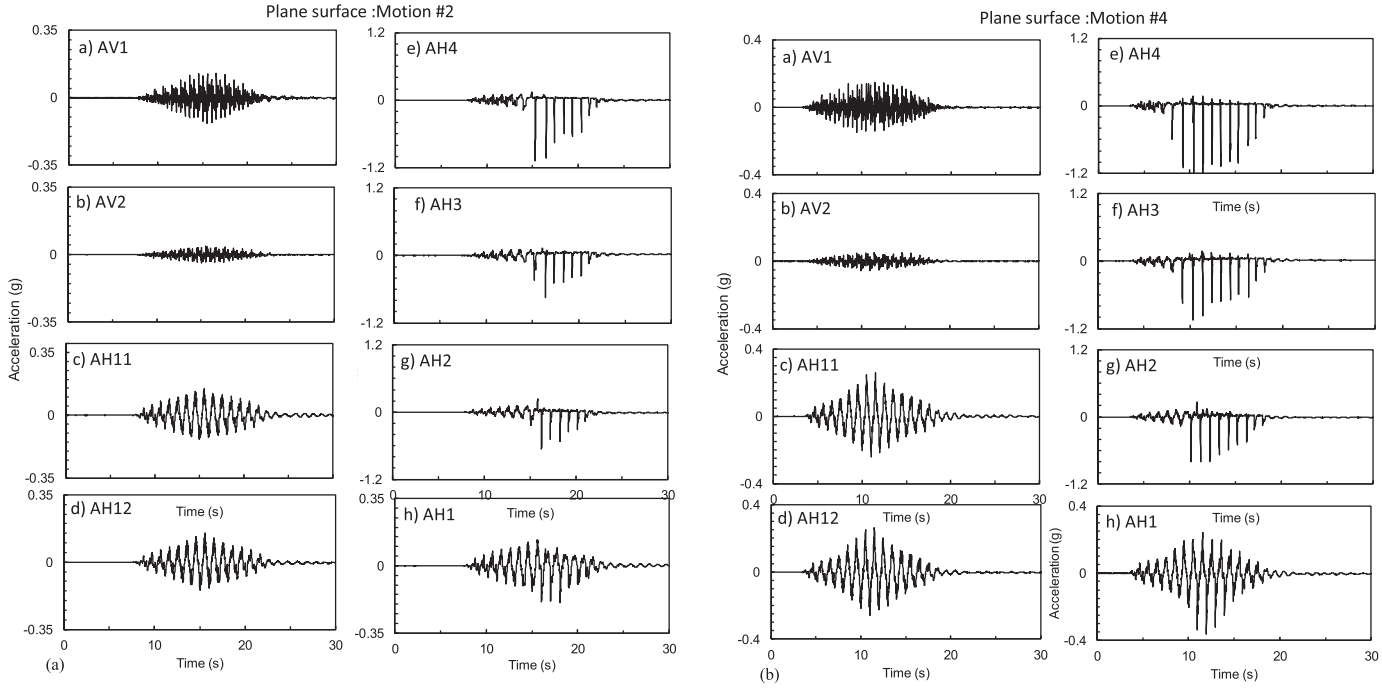

Fig. 13. (a) Recorded accelerations in Motion #2 for the plane surface model. (b) Recorded accelerations in Motion #4 for the plane surface model.

and (b). Fig. 11(a) and (b) show the model with plane surface. Fig. 12(a) and (b) show the recorded acceleration of the curved model for Motion #2 and #4, respectively. In the same manner, Fig. 13(a) and (b) show those of the plane model. The input accelerations AH11 and AH12 are also shown in each figure. In motions #2 and #4, the wave forms of the input accelerations are quite similar. This similarity can also be observed in frequency domain as shown in Fig. 14(a) for the curved model and (b) for the plane model. In all subfigures in Fig. 14, a peak at 1.0 Hz is observed and amplitudes at other frequency components are quite similar. Despite some deviations observed between AH11 and AH12 in the spectral amplitudes less than about 0.5 Hz in Fig. 14, the shaker reproduced the input horizontal acceleration within acceptable deviations. However, comparison of the vertical accelerations in Fig. 12(a) show that the amplitude of AV1 is about 7 times larger than that of AV2. The same applies to the case of the plane surface model (Fig. 13). Although true causes of this is currently unknown, fixity of AV1 on the sandbox might have had some errors. Considering that the large vertical acceleration on AV1 appeared on

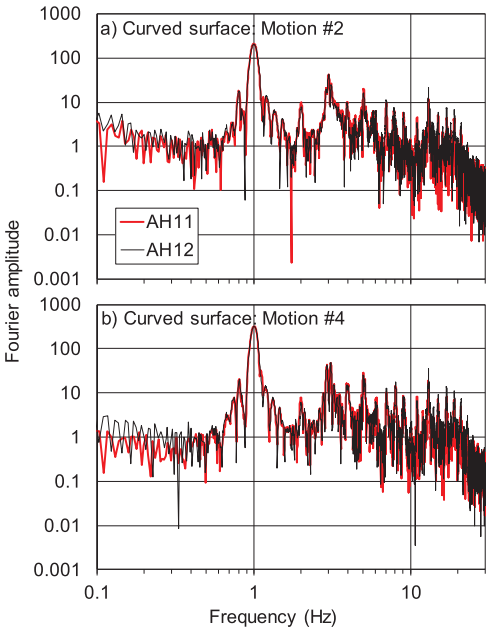

(a) Curved surface model

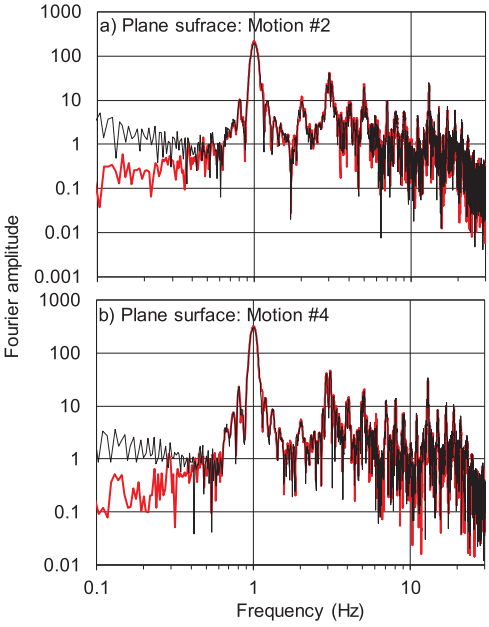

(b) Plane surface model

Fig. 14. Fourier spectra of input accelerations of Motion #2 and #4 (AH11 and AH12) for (a) curved surface model and b) plane surface model.

both the curved and plane models, the comparison of responses between them is reasonable.

By checking the horizontal acceleration responses [e) AH4, f) AH3, g) AH2 in Figs. 12 and 13], spikes with large amplitudes due to cyclic mobility induced by the lateral displacement are observed in both Motion #2 and #4. In the curved surface model (Fig. 12), these spikes are generated almost evenly in the positive and negative directions, and slightly more in the negative direction. This indicates that shear strains are large enough to cause dilatancy in the ground mostly in the downslope direction and slightly in the upslope direction. In contrast, the large spikes measured in the plane surface model appear only in the negative direction with slightly larger amplitudes than those of the

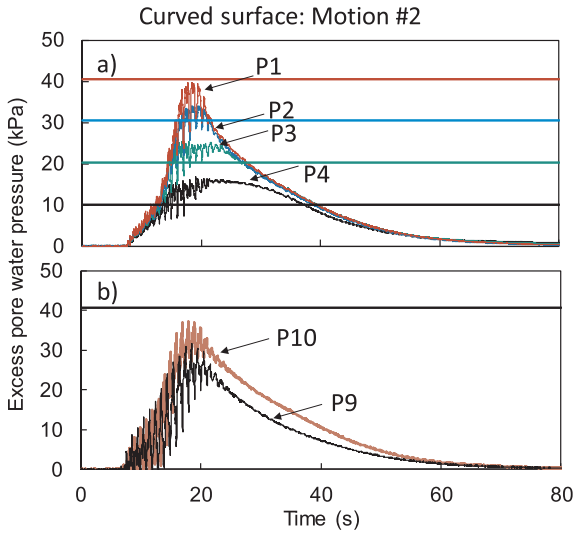

(a) Motion #2

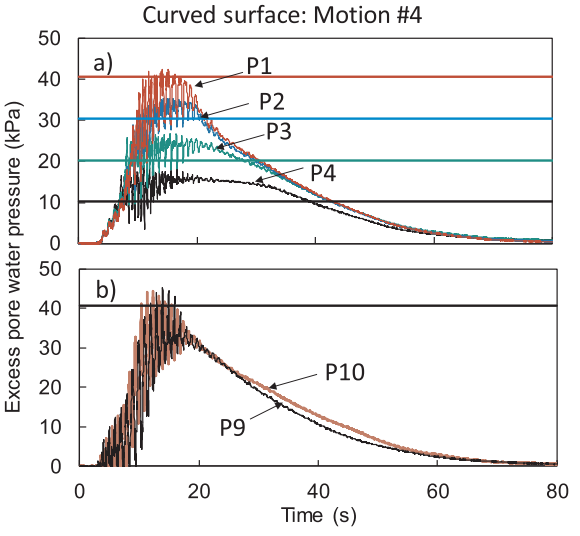

(b) Motion #4

Fig. 15. Recorded pore pressure for (a) Motion #2 and (b) Motion #4 of the curved surface model: a) P1 to P4 and b) P9-P10.

curved model [Fig. 13(a) and (b)]. This suggests that the lateral ground displacement was large enough to cause dilatancy in the plane model occurred only in the downslope direction. Fig. 10(a) of Kutter et al. [1] shows that RPI, NCU and KU are similar and have spikes due to cyclic mobility in both negative and positive directions.

Figs. 15 and 16 show the excess pore water pressures recorded at GL − 4 m (P1), − 3 m (P2), − 2 m (P3) and − 1 m (P4). In each figure, the colored horizontal lines indicate the initial effective vertical stress at the depth of the sensors (P1: Red, P2: Blue, P3 Green, and P4: Black). Excess pore water pressures of Motion #2 in the curved surface model [Fig. 15(a)] indicates that the ground was liquefied at least down to GL-3 m (P2). Excess pore water pressure at GL-4 m (P1, P9 and P10) did not reach the initial vertical effective stress. While in Motion #4, the recordings indicate that the entire ground was liquefied as recordings P1, P9 and P10 reached the initial effective vertical stress. On the other hand, for the plane surface model, the excess pore water pressures at GL − 4 m (Fig. 16) did not reach their maximum even for Motion #4. The excess pore water pressure recordings have drops that are more prominent in the plane surface model, whose mechanism should be related to the induced spikes observed in the acceleration records (Fig. 13).

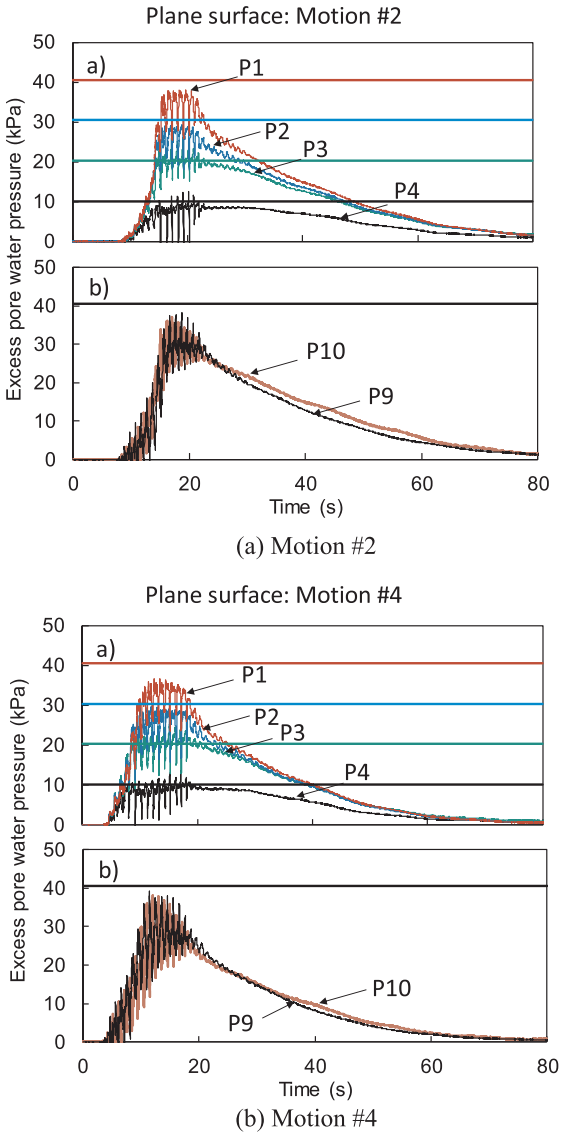

Fig. 16. Recorded pore pressure for (a) Motion #2 and (b) Motion #4 of the plane surface model: a) P1 to P4 and b) P9-P10.

For the curved surface model (Fig. 15), the maximum values of the excess pore water pressure at GL- 3 m (P2), − 2 m (P3) and − 1 m (P4) exceed the initial effective vertical stresses in both Motion #2 and #4. In contrast, the plane surface model (Fig. 16) has maximum values that appear to be bounded by the initial effective vertical stresses. The cause of this exceedance is not known; however, it should be noted that in Fig. 15 the initial overburden pressure of the top three sensors (P2 to P4) might not correspond to the actual value. When constructing the curved ground, vacuum is used to form the curvature. This process was not a usual exercise in our institute and might lead to error, and it is possible that sand was not removed properly. By using the average excess pore water pressures from 12 s to 20 s measured in the Motion #4, the depth of each sensor is back calculated as 3.5 m (P1), 3.2 m (P2), 2.3 m (P3), and 1.5 m (P4).

Fig. 17 shows images of the ground surface with markers before and after Motion #4 for the curved model [Fig. 17(a)] and for the plane model [Fig. 17(b)]. In each figure, images after the shaking are superimposed on images taken before shaking to illustrate the uniformity, magnitude and direction of displacements of the ground surface. The shown arrows indicate the direction of lateral displacement of the surface, and the dotted and solid curves connecting markers indicate

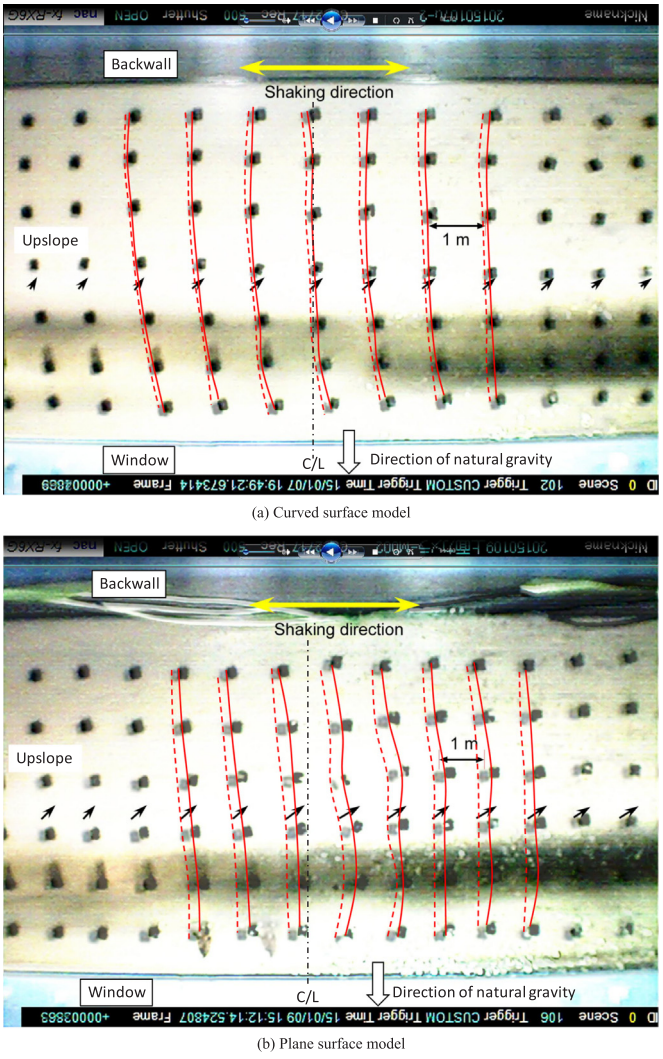

Fig. 17. Displacements of the surface markers before and after Motion #4. (a) curved surface model and (b) plane surface model.

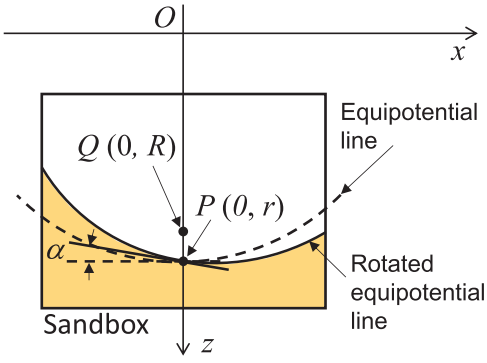

Fig. 18. Procedure to setup the curved slope ground as a rotated equipotential line.

the magnitude of displacements along the length of the sand box.

With respect to Fig. 17, the lateral displacement in the curved model [Fig. 17(a)] is significantly smaller and more uniform than that of the plane model [Fig. 17(b)]. As discussed below, this difference might be due to the variation of radial gravity acting on the model ground surfaces. In both cases, the direction of lateral displacements is in the downslope with a significant component in the direction transverse to the slope (upwards) and opposite of the direction of natural gravity.

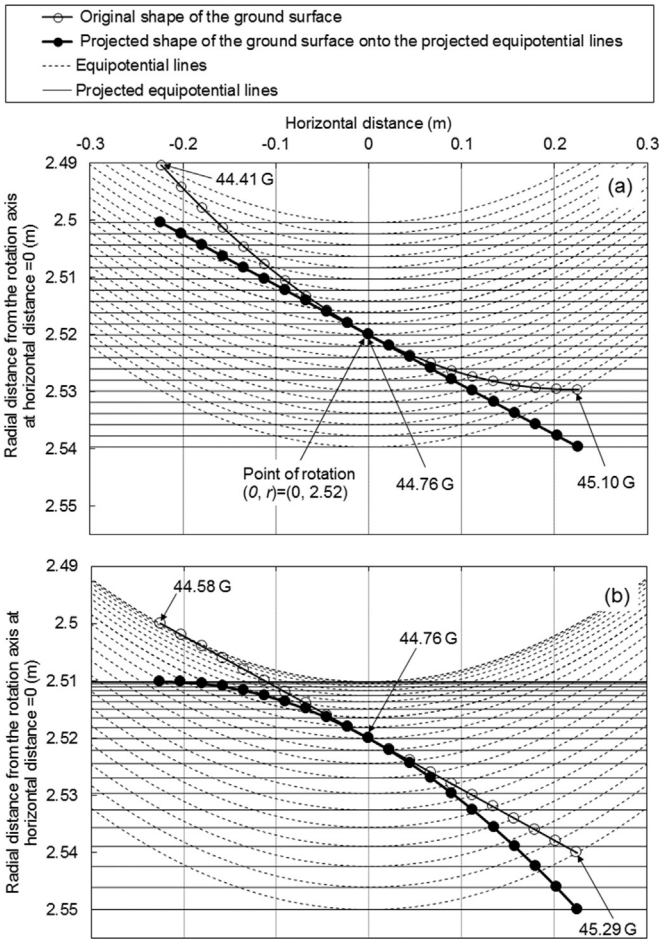

Fig. 19. Original shape and projected ground surface: (a) Curved surface and (b) Plane surface.

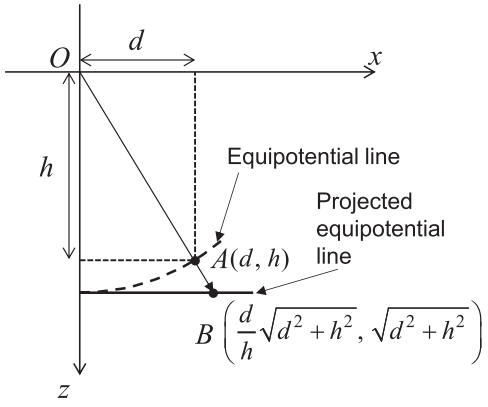

Fig. 20. Projection of points on the equipotential line.

The cause of this is as-yet-unknown. One possible cause may be the base of the model container that is not perpendicular during flight to the resultant of the centrifugal acceleration and the acceleration due to natural gravity. It may occur if there is friction in the swing mechanism. Then there could be a lateral component of the centrifugal acceleration that may cause effective inclination of the ground surface (in the transverse direction). However, the platform of the centrifuge at DPRI is supported by a set of hinges and the swing is quite smooth. Also a steel bar is attached as a balance weight at the base of the platform to keep it on the level under 1 G. Another possibility is a drag force induced by hydraulic tubes attached to the shaker, which may pull down the platform during flight. These causes should be investigated.

5. Discussion

In the LEAP-GWU-2015 experiments, a curved surface was specified by the organizer to reduce the effect of the radial gravity on the sloping ground. Construction of the curved surface in preparation for the model tests at DPRI-KU was explained above. Here, the effects of the curved surface are assessed by comparing dynamic response of the plane surface model.

In the coordinate system (x, z) defined in Fig. 18, the equipotential line which passes through a point P (0, r) is shown, where P is located at the center of the ground surface and r is the distance from the center axis of rotation to the ground surface. In the centrifuge at DPRI-KU, the centrifugal acceleration is determined as the radial acceleration at the nominal radius of rotation of $r = 2.5$ m which corresponds to the length measured from the axis of rotation to 2/3 of the sandbox's height (10 cm from the bottom of the box in model scale) to minimize the variation in confining stresses in the gravity field [2]. However, in the model testing discussed above, the centrifugal acceleration was not adjusted to be at the 1/3 of the model ground height measured from the bottom of the box.

The curved slope ground is obtained as a rotated equipotential line, as shown in Fig. 18. The surface is rotated at a point P by a slope angle α (positive in the clockwise direction) which is 5 degrees in this study. Here, the coordinates of the curved surface in the clockwise rotation with an angle α at the point P is given by Eq. (1),

$$\begin{pmatrix} x' \\ z' \end{pmatrix} = \begin{pmatrix} \cos\alpha & -\sin\alpha \\ \sin\alpha & \cos\alpha \end{pmatrix} \begin{pmatrix} x \\ z-r \end{pmatrix} + \begin{pmatrix} 0 \\ r \end{pmatrix} \tag{1}$$

as shown in Fig. 19(a) with open circles. In this study, the coordinates of the point of rotation is given by P (0, r) = (0, 2.52) as shown in Fig. 19(a). In Fig. 19, the horizontal axis is the horizontal distance from the center of the sand box, and the vertical axis is the radial distance from the rotation axis (note the different scales for the horizontal and vertical axes leading to the 5° rotation angle to appear significantly larger). Using the parameters of this study, i.e., the length of the box = 0.45 m, the curved and plane surfaces are shown, respectively as a curved segment [Fig. 19(a)] and a line segment [Fig. 19(b)] with open circles. In Fig. 19, dotted curves are equipotential lines associated with the centrifugal force applied on each point of the flat and curved surfaces. The radial gravity acting on the center of the model ground surface is computed as 44.76 G at the radius of 2.52 m. The radial gravity of the curved surface varies from 44.41 to 45.10 G, respectively, at the top and toe of the slope [Fig. 19(a)], and those of the plane surface are from 44.58 to 45.29 G at respective boundaries [Fig. 19(b)].

To investigate the effect of the radial gravity, let us transfer points on the model ground surface (shown with open circles on dotted curves in Fig. 19) to points on the horizontal lines (shown with solid circles on solid lines parallel to the x axis in Fig. 19) which correspond to the potentials associated with the centrifugal forces applied on each point. The location of solid markers is determined as follows; set a point on the equipotential line to be $A(d, h)$. Then by geometrical relationship shown in Fig. 20, the projected point B can be obtained as

$$B\left(\frac{d}{h}\sqrt{d^2+h^2},\ \sqrt{d^2+h^2}\right). \tag{2}$$

Substituting coordinates of the open circles into Eq. (2), original surfaces are projected onto the horizontal potential lines associated with the centrifugal forces applied on each point. As shown in Fig. 19(a), the curved surface with open circles is transferred into the plane surface shown with solid markers. The plane surface is transferred into the curved surface with solid markers as shown in Fig. 19(b).

In Fig. 19(a) and (b), compared with the curved model, the inclination angle of the potential curve (with solid markers) of the plane

model does not have a constant gradient and it gets steeper as it approaches the toe of the slope. That is, the radial gravity acting near the top of the plane surface model is almost constant and gradually increases towards the downslope which causes a net increase in the slope effective angle. Under such a condition, when the ground is liquefied, the bottom half of the plane model may move more toward the downslope. This is observed in Fig. 17(b) as larger displacements in the bottom half of the slope, while in Fig. 17(a) displacements of each marker are small and uniform along the length of the model with curiously more movement along the window and backwall than along the centerline. This observation may explain why larger deformation was observed in the plane model [Fig. 17(b)] with spikes only in the negative direction [Fig. 13]. However, the difference in the magnitude of displacement may also be explained to some extent by the uncertain error in the density of sand prepared by different researchers.

6. Conclusions

Details of the model construction procedure for LEAP-GWU-2015 was described for future references. As Scott [4] emphasized, the issue of quality control in physical modelling has to be clarified before moving on to a next step. With this in mind, the effect of the radial gravity was investigated by comparing the behavior of the curved surface model with that of the plane surface model. Particularly important issues derived from the series of DPRI-KU tests are as follows.

Issues related to the curved model specified by the LEAP-GWU-2015 tests:

(1) One of the vertical acceleration sensors showed very high amplitude, which was 7 times higher than the other one attached to the other top end of the sandbox.
(2) Fluid viscosity in the test (47.2–52.5 cSt) was slightly higher than the target value (44.4 cSt).
(3) The maximum values of the excess pore water pressure at GL- 2 m (P3) and − 4 m (P4) exceed the initial effective vertical stresses in both Motion #2 and #4. Considering that measured excess pore pressures exceed the specified overburden, it is possible that sand was not be removed properly with the employed vacuum. By using the maximum excess pore water pressures measured in the Motion #4, the depth of each sensor is back calculated as 4.2 m (P1), 3.5 m (P2), 2.7 m (P3), and 1.9 m (P4).

Issues related to the radial gravity:

(1) In the curved surface model, spikes on acceleration records appear almost evenly in the positive and negative directions, and slightly more in the negative direction. In contrast, the large spikes on acceleration measured in the plane surface model appear only in the negative direction with slightly larger amplitudes than those of the curved model. Similarity may be found in Fig. 10(a) of Kutter et al. [1]. RPI, NCU and KU have spikes due to cyclic mobility in both negative and positive directions.
(2) In the excess pore water pressure recordings, spikes in the negative direction are more prominent in the plane surface model; the spikes in pore pressure should be related to the induced spikes observed in the acceleration records.
(3) Larger lateral displacement in the bottom half of the slope was observed in the plane model, while in the curved model, displacements of each marker are smaller and uniform along the length of the model with curiously more movement along the window and backwall than along the centerline. In the plane model, the radial gravity acting near the top of the slope is almost constant and gradually increases towards the toe of the slope, which might cause a net increase in the slope effective angle.

The comparison of the ground motions between the curved and plane surface models confirmed the importance of curving the model ground surface.

Acknowledgements

This research was partially supported by the Ministry of Education, Culture, Sports, Science and Technology (MEXT), Grant-in-Aid for Scientific Research (B) (26282103, 2014–2016), and Grant-in-Aid for Scientific Research (C) (25420502, 2013–2015). The authors also thank Dr. Shuji Tamura at Tokyo Institute of Technology, Japan, for permission to use the mold to create the curved surface.

References

[1] Kutter BL, Carey TJ, Hashimoto T, Zeghal M, Abdoun T, Kokkali P, et al.. LEAP-GWU-2015 Experiment Specifications, Results, and Comparisons. Soil Dynamics and Earthquake Engineering, This issue; 2016.
[2] Madabhushi G. Centrifuge modelling for civil engineers. Boca Raton, London, New York: CRC Press. Taylor & Francis Group; 2014. p. 292.
[3] Okamura M, Inoue T. Preparation of fully saturated model ground. Arulanandan K, Scott RF, editors. Physical modelling in geotechnics, 1. London: Taylor & Francis Group; 2010. p. 147–52.
[4] Scott RF. Lessons learned from VELACS project. In: Proceedings of the international conference on the verification of numerical procedures for the analysis of soil liquefaction problems, Vols. 1 & 2. A. A. Balkema; 1994. p. 1773–79.